Microsyst Technol (2012) 18:1–8
DOI 10.1007/s00542-011-1380-1

TECHNICAL PAPER

# $Bi_2Te_3$-$Sb_2Te_3$ on polymeric substrate for X-ray detectors based on the seebeck effect

**J. G. Rocha · L. M. Goncalves · S. Lanceros-Mendez**

Received: 5 January 2011 / Accepted: 9 November 2011 / Published online: 23 November 2011


**Abstract** A theoretical and experimental basis for a x-ray detector concept, based on the conversion of x-rays into thermal energy is presented. The detector follows an indirect approach: the x-rays are first converted into thermal energy, which is then converted into electrical signals by the Seebeck effect. The detector does not need high operating voltages as the detectors based on photoconductors, it shows higher efficiency in energy conversion than x-ray detectors based on scintillators and it has a better intrinsic signal to noise ratio than both photoconductor and scintillator methods. Moreover, this technique allows the fabrication of x-ray detectors on polymeric substrates, which is not so viable with the other aforementioned methods. As a drawback, the frequency response of this detector is usually low. This drawback can be overcome by reducing the mass of the detector.

## 1 Introduction

X-rays can be converted into electrical signals by two main approaches, known as direct and indirect methods (Rocha et al. 2009). Independently of the used method, to achieve an x-ray image (e. g. radiography or tomography) it is necessary to place many x-ray detectors in an array disposition. In the direct method, the x-ray detectors are usually based in photoconductors. In the indirect method, scintillators associated to photodetectors are typically used. Each x-ray detection method has its performance advantages and limitations on its use for practical x-ray image detectors.

The direct method based on photoconductors uses photoconductive materials with high x-ray absorption capability. These materials can be placed on an array of conductive charge collection plates, each of them supplied with a storage capacitor. There are some devices based on photoconductors such as CdTe, CdZnTe, $HgI_2$ and $PbI_2$ (Zentai et al. 2005; Abbene et al. 2009; Watanabe et al. 2009). The readout electronic circuitry must be developed in a separate die due to incompatibilities between the two fabrication processes. Moreover, for the operation of these devices, a high-voltage is necessary for biasing the photoconductors.

The indirect method uses materials that absorb x-rays and convert their energy into visible light, which is easily detected by silicon photodetectors, for example (Rocha et al. 2004; Martin et al. 2009). These materials, known as scintillators, usually consist on compounds constituted by elements of high atomic number, which have high x-ray absorption capability, and yield many visible light photons for each absorbed x-ray quantum. The main drawback of this configuration is its low energy efficiency, especially for detectors with small dimensions or detector arrays with small pixel sizes (Rocha and Lanceros-Mendez 2006). This low efficiency is due to large losses in the energy conversion both from x-rays to visible light and from visible light to electrical current.

## 2 Theoretical analysis

To avoid the previously presented drawbacks of the other commonly used x-ray detectors, this work shows a device

J. G. Rocha (✉) · L. M. Goncalves
Algoritmi Research Center, University of Minho,
Campus de Azurem, 4800-058 Guimaraes, Portugal
e-mail: gerardo@dei.uminho.pt

S. Lanceros-Mendez
Center of Physics, University of Minho,
Campus de Gualtar, 4710-057 Braga, Portugal

based on thermal effects. The increase in efficiency is achieved by converting the x-rays into thermal energy, which is then detected by means of the Seebeck effect. Moreover, with this technique it will be possible to fabricate x-ray detectors on polymeric substrates, as it will be demonstrated in this article.

The working principle of the x-rays detector based on the Seebeck effect consists in detecting the increase in temperature caused by the absorption of the x-rays by a material with high atomic number and high-density. A junction of two materials with different Seebeck coefficients is used to detect the increase in temperature.

The theoretical analysis of the detector can be divided into three sections: the production of x-rays, its absorption by the plate and the detection of temperature changes.

### 2.1 X-ray source

The efficiency of the x-ray production can be defined as the rate of kinetic energy of the electrons that is converted into x-rays. The efficiency $\eta$ is directly proportional to the atomic number of the material used as anode in the x-ray source ($Z$) and to the electrical potential difference between the anode and the cathode ($V$), usually in the range from 10 to 120 kV:

$$\eta = KZV \tag{1}$$

where $K \approx 1 \times 10^{-6}\,\mathrm{V}^{-1}$ (Selman 1994). Disregarding relativistic effects, the x-ray power is given by:

$$P_{\mathrm{rx}} = \eta VI \tag{2}$$

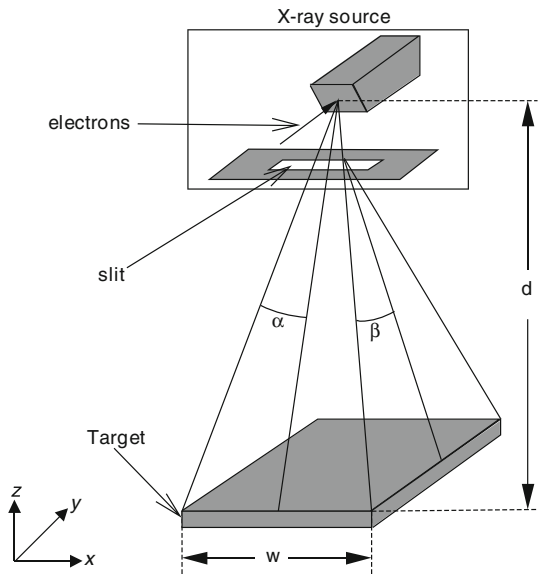


**Fig. 1** Angles at which the x-rays can be absorbed by the target

where $VI$ is the input electrical power of the x-ray tube.

Figure 1 shows a target placed in the plane of the x-rays at a distance $d$ from the x-ray source.

The maximum angle $\alpha$ at which the x-rays can be absorbed by the target can be obtained from:

$$\alpha = \arctan\frac{w}{2d}. \tag{3}$$

As the x-rays are produced randomly in the tube, with equal probability in any direction perpendicular to the beam of electrons that originates them, the ratio between the x-rays arriving at the target and the ones that are produced by the source is $\alpha/\pi$.

The power of the x-rays arriving at the target will be

$$P_{\mathrm{tg}} = \frac{\alpha P_{\mathrm{rx}}}{\pi}. \tag{4}$$

The former calculation has been performed in one dimension, once the scattering produced by the slit and the relativistic effects do not produce significant changes in x-ray distribution in distribution in $y$ direction, for small values of $d$.

### 2.2 Absorption of x-rays

When penetrating into a material layer, a beam of x-rays is absorbed according to an exponential law:

$$I = I_o e^{(-\mu/\rho)\rho x} \tag{5}$$

where $I_0$ is the initial intensity of the beam, $I$ is its intensity at a distance $x$ from the surface and $\rho$ is the density of the material. The ratio $(\mu\rho)$ is the mass absorption coefficient of the material and can be found in tables like the one published by (Hubbell 1982).

### 2.3 Conversion of x-ray energy into heat and detection of temperature changes

The x-rays that are absorbed by the target material of the detector will heat it. The corresponding temperature change can be calculated from:

$$Q = c\,m\frac{dT}{dt} \tag{6}$$

where $Q$ is the energy of the absorbed x-rays, $c$ and $m$ are the specific heat capacity and the mass of the target material and $dT/dt$ is the time change ratio of temperature. In order to stop and absorb the x-ray energy it is necessary a material with high atomic number and density (Eq. 5). On the other hand, to obtain higher temperature changes, it is more appropriate a material with low mass and low specific heat capacity (Eq. 6).

### 2.4 Experimental validation of the working principle

In order to validate the theory, a simple detector, constituted by a copper plate and a K type thermocouple was built. The x-ray source used in the experiments works with a voltage of 35 kV and a current that can range from 0 to 1 mA, which means that the maximum electrical power absorbed by the x-ray source is 35 W. The efficiency of the x-ray production, given by Eq. 1, for an x-ray source with molybdenum anode ($Z = 42$) and an electrical voltage of 35 kV, is approximately equal to $1.47 \times 10^{-3}$. As a result, the power of the produced x-rays is 51.45 mW (Eq. 2).

In Fig. 1, the target has $w = 1$ mm and it is placed in the plane of the x-rays at a distance $d = 10$ cm from the x-ray source. The maximum angle $\alpha$ at which the x-rays can be absorbed by the target, given by Eq. 3 is $\alpha = 5 \times 10^{-3}$ rad.

The power of the x-rays arriving at the target will be 88.89 μW (Eq. 4).

When penetrating into a material layer, a beam of x-rays is absorbed according to the exponential law of Eq. 5. Applying Eq. 5 to a copper plate of 0.2 mm of thickness, it is possible to calculate that 99.739% of the incident x-ray photons of 20 keV of energy (which is approximately the energy peak produced by a 35 kV x-ray tube) will be absorbed. Figure 2 shows a simulation graph of the percentage of x-rays absorbed by a copper plate as a function of its thickness and Fig. 3 shows a simulation graph of the percentage of x-rays absorbed by a 200 μm copper plate as a function of the incident x-ray energy.

Table 1 shows the atomic number, the density and the specific heat capacity of some metals.

With the data of Table 1, by performing some calculations, it is possible to conclude that copper is a material that better satisfies the requirements expressed by Eqs. 5 and 6.

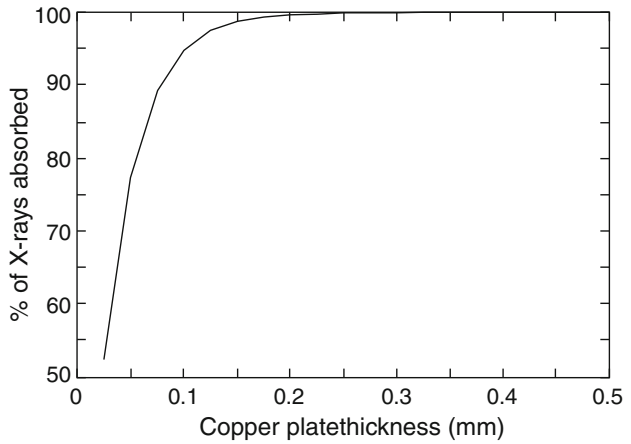


**Fig. 2** Percentage of 20 keV x-ray photons absorbed by a copper plate as a function of the plate thickness

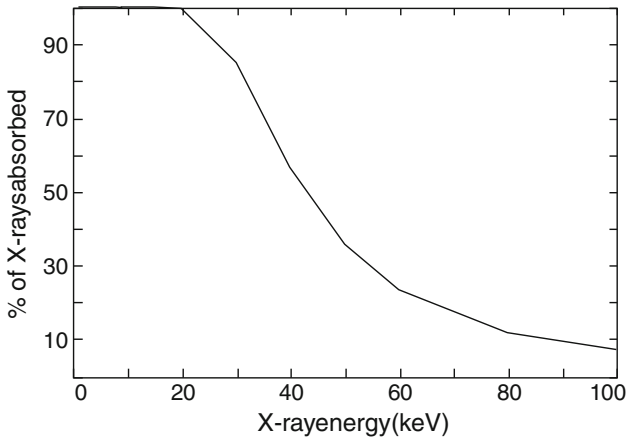


**Fig. 3** Percentage of x-rays absorbed by a 200 μm copper plate as a function of the incident x-ray energy

**Table 1** Atomic numbers, densities and specific heat capacities of some metals at 300 K (Schumm et al. 1973)

| | Atomic number | Density (g cm$^{-3}$) | Specific heat capacity (J g$^{-1}$ K$^{-1}$) |
|---|---|---|---|
| Aluminum | 13 | 2.7 | 0.897 |
| Iron | 26 | 7.8 | 0.450 |
| Copper | 29 | 8.96 | 0.385 |
| Silver | 47 | 10.5 | 0.235 |
| Platinum | 78 | 21.4 | 0.135 |
| Gold | 79 | 19.3 | 0.1291 |
| Lead | 82 | 11.3 | 0.125 |

A copper target has a specific heat capacity of 0.385 J g$^{-1}$K$^{-1}$ and a density of 8.96 g cm$^{-3}$ at 300 K. If the target has a volume of 0.2 mm$^3$, its mass is 1.792 mg.

The energy of the x-rays that is absorbed by the copper plate during 1 s is 81.88 μJ and the temperature change would be equal to 118.7 mK. At this point we have neglected the effect of the power dissipation by convection and thermal radiation of the target.

A type K thermocouple produces a potential difference of 39.7 μV/K, for small temperature differences between hot and cold junctions. In this case, the temperature of 118.7 mK will produce a voltage of 4.711 μV. This is the order of magnitude of the values expected in the first experiments, where the results are in Fig. 4.

As it can be observed in the figure, the measured values are lower than the expected ones. This can be explained mainly with the power dissipation of the detector and thermal losses through the substrate and thermocouple wires. By coating the detector target with a low-density thermal insulating material, the dissipation can be reduced. Small dimensions of thermocouple wires can also reduce

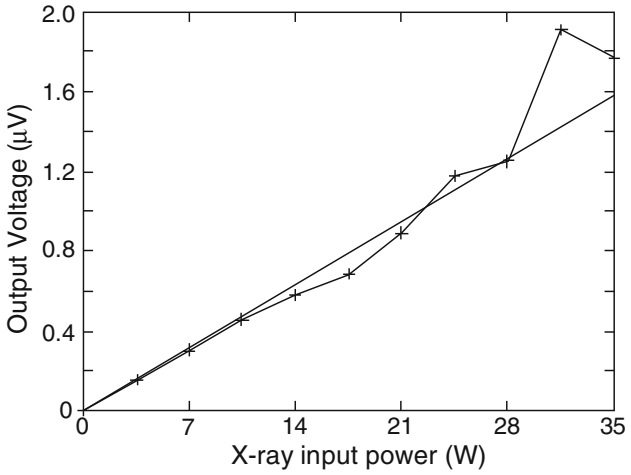


**Fig. 4** Measurements obtained with the test device: The x-ray tube was powered with a voltage of 35 kV and a current ranging from 0 to 1 mA (input power ranging from 0 to 35 W)

thermal losses. It can also be observed in Fig. 4 that there is a linear relationship between the output voltage generated in the thermocouple and the x-ray input power. This experiment proved nevertheless that the working principle of the detector is valid.

## 3 Comparison between methods

The most common noise sources in pixel detectors for x-ray imaging systems are photonic noise, fixed pattern noise, and readout electronics noise (Workman and Brettle 1997). The fixed pattern noise is a characteristic of all pixel array sensors and can be canceled by the use of gain maps (Tate et al. 1995). The noise of the readout electronics depends mainly on the circuit configuration and layout and usually is less important than the photonic noise in the x-ray spectrum. The photonic noise, which is caused by the statistical distribution of the x-ray photons in time and space, is the fundamental noise limit of an x-ray detector. Several theoretical analysis and experiments have shown that the intrinsic photonic noise of an x-ray beam is random and follows a Poisson distribution; that is, the standard deviation $\sigma_{\text{prx}}$ is equal to the square root of the average number of x-ray photons $m_{\text{prx}}$ (Workman and Brettle 1997; Tate et al. 1995), such that:

$$\sigma_{\text{prx}} = \sqrt{m_{\text{prx}}} \tag{7}$$

and the signal to noise ratio (SNR) is given by:

$$\text{SNR} = \frac{m_{\text{prx}}}{\sigma_{\text{prx}}} = \sqrt{m_{\text{prx}}}. \tag{8}$$

### 3.1 Detectors based on scintillators

A scintillator converts the absorbed energy into visible light. In the case of the CsI:Tl, a very common scintillator, it produces about 65,900 visible photons for each 1 MeV of absorbed energy, at room temperature (Valentine et al. 1991), that is, for each photon of 1 MeV, it produces a random number of photons whose average is 65,900. By the other hand, the scintillators usually are coated by layers materials in order to guide the visible light produced by them to the photodetectors. Therefore, the average amount of produced light for a given x-ray energy, $L_{\text{R}}(E)$, is obtained by the product of five factors, namely (a) the number of incident x-ray photons $m_{\text{prx}}$, which is a random quantity; (b) the transmissivity of the reflective layer on top of the scintillator, $\text{Tr}_{\text{ref}}$ that the x-rays must cross; (c) the absorption of the scintillator, $\text{Ab}_{\text{sc}}$; (d) the number of visible photons per MeV ($N_{\text{vph/Mev}}$) produced by the scintillator, which is the mean value of a random process; and (e) the energy of each x-ray photon, $E$. Thus:

$$L_{\text{R}}(E) = m_{\text{prx}}\text{Tr}_{\text{ref}}\text{Ab}_{\text{sc}}N_{\text{vph/MeV}}E \tag{9}$$

In this case, the variance of the produced photon distribution, $\sigma^2_{\text{LR}}(E)$, is given by the product of the mean value of the photons absorbed by the scintillator and the square of the number of visible photons produced in the scintillator for each incident x-ray photon, such that:

$$\sigma^2_{\text{LR}}(E) = m_{\text{prx}}\text{Tr}_{\text{ref}}\text{Ab}_{\text{sc}}\left(N_{\text{vph/MeV}}E\right)^2. \tag{10}$$

This result is in accordance with previously presented works (Gruner et al. 2002; Swank 1973).

The Signal to Noise Ratio (SNR) is given by

$$\text{SNR}_{\text{sc}}(E) = \frac{L_{\text{R}}(E)}{\sigma_{\text{LR}}(E)} = \sqrt{m_{\text{prx}}\text{Tr}_{\text{ref}}\text{Ab}_{\text{sc}}} \tag{11}$$

When the incident x-ray photons follow a Poisson distribution, the losses introduced by the detection system affect in the same way both the mean and the variance of the distribution, that is, the electron–hole pairs created in the photodetector also follow a Poisson distribution.

Nevertheless, due to the randomness of the process of production of visible light in the scintillator, the visible photons do not follow a Poisson distribution. It can be modeled by a Normal distribution with mean $m_{\text{sc}}$ and variance $\sigma^2_{\text{sc}}$. In this case, the losses can be explained by a Binomial distribution whose probability of success (the photon generates an electron–hole pair) is $p$. The distribution of electron–hole pairs in the photodetector is obtained by multiplying the distribution of the light produced by the scintillator by this binomial distribution. The resulting mean is:

$$m_{\mathrm{ehp}}(E) = p\,L_{\mathrm{R}}(E) \tag{12}$$

and the variance is (Gordon and Gordon 1994):

$$\sigma^2_{\mathrm{ehp}}(E) = p(1-p)L_{\mathrm{R}}(E) + p^2\sigma^2_{\mathrm{LR}}(E), \tag{13}$$

which gives:

$$\mathrm{SNR}_{\mathrm{ehp}}(E) = \frac{p\,m_{\mathrm{prx}}\mathrm{Tr}_{\mathrm{ref}}\mathrm{Ab}_{\mathrm{sc}}N_{\mathrm{vph/MeV}}E}{\sqrt{p\,m_{\mathrm{prx}}\mathrm{Tr}_{\mathrm{ref}}\mathrm{Ab}_{\mathrm{sc}}N_{\mathrm{vph/MeV}}E\left(1+p\left(N_{\mathrm{vph/MeV}}E-1\right)\right)}} \tag{14}$$

Finally, the fact that some x-ray photons cross completely the scintillator and are absorbed by the photodetector will also decrease the signal to noise ratio.

### 3.2 Detectors based on photoconductors

The average amount of produced electron–hole pairs in a photoconductor, for a given x-ray energy, $eh(E)$, is obtained by the product of four factors, namely (a) the number of incident x-ray photons $m_{\mathrm{prx}}$, which is a random quantity; (b) the absorption of the photoconductor, $\mathrm{Ab}_{\mathrm{ph}}$; (c) The number of electron–hole pairs per MeV ($N_{\mathrm{ehp/MeV}}$) produced by the photoconductor, which is the mean value of a random process; and (d) the energy of each x-ray photon, $E$. Thus:

$$eh(E) = m_{\mathrm{prx}}\mathrm{Ab}_{\mathrm{ph}}N_{\mathrm{ehp/MeV}}E \tag{15}$$

In this case, the variance of the produced photon distribution, $\sigma^2_{\mathrm{eh}}(E)$, is given by the product of the mean value of the photons absorbed by the photoconductor and the square of the number of electron–hole pairs produced for each incident x-ray photon, such that:

$$\sigma^2_{\mathrm{eh}}(E) = m_{\mathrm{prx}}Ab_{\mathrm{ph}}\left(N_{\mathrm{ehp/MeV}}E\right)^2. \tag{16}$$

The SNR for each energy is given by:

$$\mathrm{SNR}_{\mathrm{ph}}(E) = \frac{eh(E)}{\sigma_{\mathrm{eh}}(E)} = \sqrt{m_{\mathrm{prx}}Ab_{\mathrm{ph}}} \tag{17}$$

### 3.3 Detector based on thermal effects

The average amount heat produced for a given x-ray energy, $h(E)$, is obtained by the product of five factors, namely (a) the number of incident x-ray photons $m_{\mathrm{prxt}}$, which is a random quantity; (b) the transmissivity of a thermal insulating layer on top of the detector, $\mathrm{Tr}_{\mathrm{ins}}$ that the x-rays must cross; (c) the absorption of the detector plate, $\mathrm{Ab}_{\mathrm{pl}}$; (d) the energy of each x-ray photon $E$; and (e) a conversion factor of x-ray energy into heat, $k$. Thus:

$$h(E) = m_{\mathrm{prxt}}\mathrm{Tr}_{\mathrm{ins}}\mathrm{Ab}_{\mathrm{pl}}E\,k \tag{18}$$

In this case, the variance of the produced photon distribution, $\sigma^2_{\mathrm{h}}(E)$, is given by:

$$\sigma^2_{\mathrm{h}}(E) = m_{\mathrm{prxt}}\mathrm{Tr}_{\mathrm{ins}}\mathrm{Ab}_{\mathrm{pl}}E\,k. \tag{19}$$

The SNR for each energy is given by:

$$\mathrm{SNR}_{\mathrm{h}}(E) = \frac{h(E)}{\sigma_{\mathrm{h}}(E)} = \sqrt{m_{\mathrm{prxt}}\mathrm{Tr}_{\mathrm{ins}}\mathrm{Ab}_{\mathrm{pl}}E\,k}. \tag{20}$$

In order to compare the previously presented results (Eqs. 14, 17 and 20), we can calculate the minimum detectable number of x-ray photons by each method, which happens when the corresponding SNR is equal to 1.

For the detector based on scintillators, making $\mathrm{SNR}_{\mathrm{ehp}}(E) = 1$ in Eq. 14 and solving for $m_{\mathrm{ehp}}(E)$, gives:

$$m_{\mathrm{ehp\,min}}(E) = \frac{1-p}{p\,\mathrm{Tr}_{\mathrm{ref}}\mathrm{Ab}_{\mathrm{sc}}N_{\mathrm{vph/MeV}}E} + \frac{1}{\mathrm{Tr}_{\mathrm{ref}}\mathrm{Ab}_{\mathrm{sc}}}. \tag{21}$$

As $\mathrm{Tr}_{\mathrm{ref}}$, $\mathrm{Ab}_{\mathrm{sc}}$ and $p$ are always in the interval from 0 to 1, $m_{\mathrm{ehp\,min}}(E)$ is always higher than 1.

For the detector based on photoconductor, making $\mathrm{SNR}_{\mathrm{ph}}(E) = 1$ in Eq. 17 and solving for $m_{\mathrm{prx}}(E)$, gives:

$$m_{\mathrm{prx\,min}}(E) = \frac{1}{\mathrm{Ab}_{\mathrm{ph}}}. \tag{22}$$

Like in the previous case, as $\mathrm{Ab}_{\mathrm{ph}}$ is in the interval from 0 to 1, $m_{ehp\,\mathrm{min}}(E)$ is always higher than 1.

Finally, for the detector based on thermal effects, making $\mathrm{SNR}_{\mathrm{h}}(E) = 1$ in Eq. 20, and solving for $m_{\mathrm{prxt}}(E)$, gives:

$$m_{\mathrm{prxt\,min}}(E) = \frac{1}{\mathrm{Tr}_{\mathrm{ins}}\mathrm{Ab}_{\mathrm{pl}}E\,k} \tag{23}$$

In this case, the quantity $\mathrm{Tr}_{\mathrm{ins}}\mathrm{Ab}_{\mathrm{pl}}E\,k$ can be higher than 1 and the minimum detectable number of x-ray photons is 1 photon.

## 4 Fabrication of the detector

After the positive result in the previous experiment, described in sect. 2, an x-ray detector was fabricated on a flexible polyimide Kapton© substrate.

Thermoelectric p-type ($Sb_2Te_3$) and n-type ($Bi_2Te_3$) thin films with thickness of 5 μm with high figures of merit were obtained by a thermal co-evaporation method (Goncalves et al. 2006) in a high-vacuum chamber with base pressure $p = 3 \times 10^{-6}$ mbar. The substrate temperature and evaporation rates were controlled during all the deposition process in order to obtain the desired properties. The power applied to each boat was controlled independently, using two PID (Proportional Integral and Derivative) controllers in order to maintain the deposition rate at a fixed value, different for each material. The Bi or Sb

**Table 2** Summary of the thermoelectric properties of $Bi_2Te_3$ and $Sb_2Te_3$

| Film | Te (%) | Bi or Sb (%) | Seebeck ($\mu V\ K^{-1}$) | Resistivity ($\mu\Omega$ m) | Fig. Merit (300 K)[a] |
|---|---|---|---|---|---|
| $Bi_2Te_3$ | 62 | 38 | −248 | 12.6 | 0.86 |
| $Sb_2Te_3$ | 73 | 27 | 188 | 12.6 | 0.49 |

[a] Thermal conductivity of 1.7 $Wm^{-1}\ K^{-1}$ was assumed on calculations

evaporation flow rate was maintained at 2 Å $s^{-1}$, and the Te evaporation flow rate at 6 Å $s^{-1}$.

The device was fabricated on a 50 μm polyimide substrate. Metal pads (1 μm of aluminium covered with 20 nm of nickel) were evaporated through a metal mask. On top of contacts, 1 μm-thick bismuth telluride and antimony telluride films were deposited, also through metal masks, resulting in two thermoelectric legs. Seebeck coefficients of 220 and 180 $\mu V \cdot K^{-1}$ and electrical resistivity in the range 10–20 $\mu\Omega$ m were measured on n-type and p-type films, respectively. The thermoelectric properties obtained make these materials suitable for the fabrication of sensing elements. Table 2 summarizes the thermoelectric properties, namely the Seebeck coefficient, the resistivity and the figure of merit (ZT) at 300 K, which is defined as:

$$ZT = \frac{\alpha^2}{\rho\lambda} T \tag{24}$$

where $\alpha$ is the Seebeck coefficient, $\rho$ the electrical resistivity, $\lambda$ the thermal conductivity and $T$ the temperature (Min and Rowe 1999).

Electrical resistivity, carrier concentration and Hall mobility were measured at room temperature using the conventional four probe van der Pauw geometry in a 5 mm side square arrangement. A DC magnetic field of 80 mT was applied for Hall measurements. The Seebeck coefficient, $\alpha$, was measured by connecting one side of the film to a heated metal block at a fixed temperature and the other side to a heat sink kept at room temperature, with a temperature difference between both sides below 10°C. Thermal conductivity was measured using the technique developed in (Völklein and Balles 1992).

The thermoelectric elements were connected to metal contacts, fabricated on the substrate by deposition of a 800 nm layer of aluminum covered with a thin layer of Nickel (20 nm). Thermoelectric films were deposited on the top of the contacts. These films were patterned during the evaporation process using shadow masks. In this way a thermoelectric device was fabricated.

Polyimide was chosen as substrate because of its low thermal conductivity (0.16 $Wm^{-1}K^{-1}$), thus allowing higher performance of the devices, even with higher values of substrate thickness (50 μm foil was used). Finally, a copper plate of 100 μm was placed on top of the thermoelectric materials (Fig. 5).

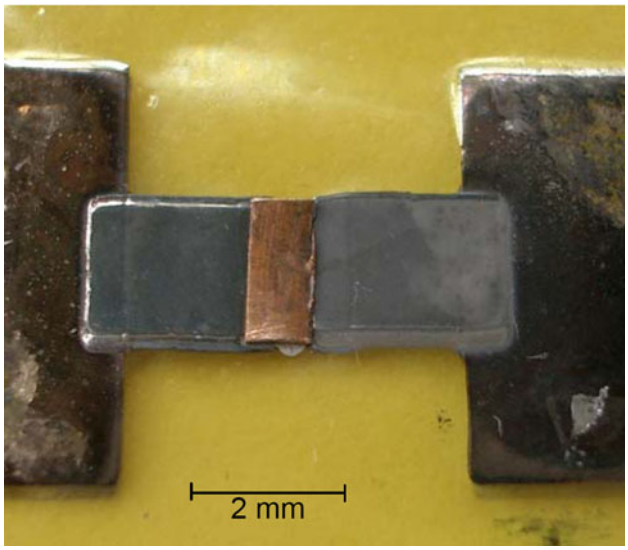


**Fig. 5** Picture of the fabricated device

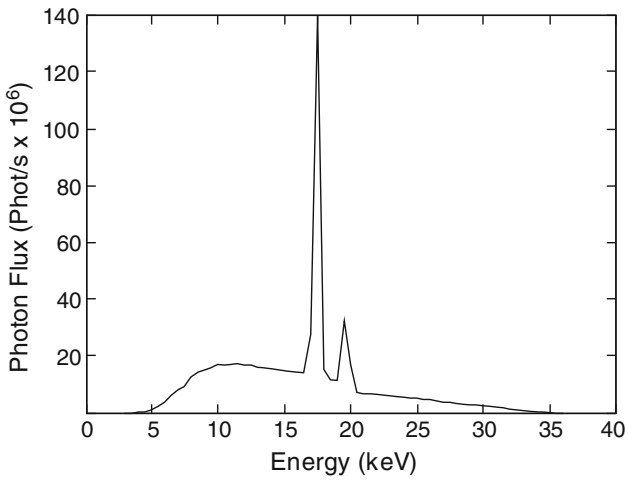


**Fig. 6** Spectrum of the radiation produced by an x-ray tube with a molybdenum anode and 35 kV × 1 mA of input power, measured with a detector of 1 $mm^2$ area, at 0.5 m from the anode

## 5 Experimental results

In order to verify experimentally the performance of the flexible fabricated device, an x-ray tube with molybdenum anode was powered with a voltage of 35 kV and a current that can range from 0 to 1 mA. Figure 6 shows the spectral distribution of such x-ray tube (Boone et al. 1997).

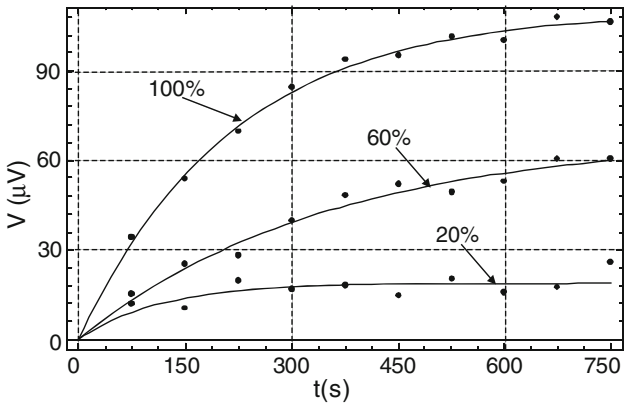


**Fig. 7** Voltages measured at the detector terminal for x-ray tube currents of 0.2, 0.6 and 1 mA, which correspond to 20, 60 and 100% of the maximum x-ray power produced by the tube

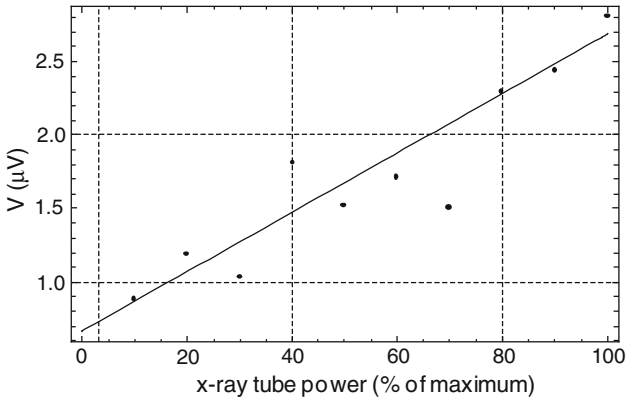


**Fig. 8** Output voltage of the detector when the input power increases

In the first experiment, the detector was placed in the x-ray path and the output voltage, which is proportional to the temperature change, was measured. Tube currents of 0.2, 0.6 and 1 mA were used, which correspond to 20, 60 and 100 of the maximum x-ray power produced by the tube. The result of this experiment is shown in Fig. 7. This figure also shows the best fit for each set of points, which are functions of the type $v(t) = v_{\max}(1 - e^{-\alpha t})$.

The obtained statistical factors $R^2$ were 0.966023, 0.99673 and 0.999512, for 20, 60 and 100% curves, respectively.

In the second experiment, the x-ray tube was powered from 0 to its maximum by changing the current in steps of 0.1 mA. The result is in Fig. 8. In this experiment, the x-rays hit the plate of the detector during 1 s. The exposure time control in our x-ray setup is manual, which can justify some experimental errors. Nevertheless, if the point obtained at 70% of the x-ray power was disregarded, the behavior of the detector is approximately linear, with a statistical factor $R^2$ of 0.927685.

## 6 Conclusions

In the present work, the Seebeck effect was used in the detection and measurement of x-ray signals. The constructed device does not need high-bias voltages to work properly as in the case of the photoconductors and it shows larger energy conversion efficiency than the detectors based on scintillating crystals. Moreover, it was fabricated on a polymeric substrate, adding interest for potential applications. Since the working principle of the detector is based on temperature changes, the main drawback of this approach is the low frequency response. However, this could be overcome by fabricating sensors with smaller dimensions, as the temperature change is inversely proportional to the mass of the detector. Active cooling by Peltier effect on the thermoelectric sensors elements can also improve the performance of the sensor and is being studied.

**Acknowledgments** This work is funded by national funds by FCT-Fundação para a Ciência e a Tecnologia, project reference PTDC/CTM-NAN/121038/2010. J. G. Rocha which to thanks to FCT for the Grant SFRH/BSAB/1014/2010.

## References

Abbene L, Del Sordo S, Caroli E, Gerardi G, Raso G, Caccia S, Bertuccio G (2009) Hard x-ray response of pixellated CdZnTe detectors. J Appl Phys 105:124508–124517

Boone JM, Fewell TR, Jennings RJ (1997) Molybdenum rhodium and tungsten anode spectral models using interpolating polynomials with application to mammography. Med Phys 24:1863–1874

Goncalves LM, Couto C, Correia JH, Alpuim P, Min G, Rowe DM (2006) Optimization of thermoelectric thin films deposited by co-evaporation on plastic substrates. Proc ICT 2006. Cardiff, UK

Gordon SP, Gordon FS (1994) Contemporary statistics—a computer approach. McGraw-Hill, Singapore

Gruner SM, Tate MW, Eikenberry EF (2002) Charge coupled device area X-ray detectors. Rev Sci Instrum 73:2815–2842

Hubbell JH (1982) Photon mass attenuation and energy-absorption coefficients from 1 keV to 20 MeV. Int J Appl Radiat Isot 33:1269–1290

Martin T, Douissard PA, Couchaud M, Cecilia A, Baumbach T, Dupre K, Rack A (2009) LSO-based single crystal film scintillator for synchrotron-based hard X-ray micro-imaging. IEEE Trans Nucl Sci 56:1412–1418

Min G, Rowe DM (1999) Cooling performance of integrated thermoelectric micro-cooler. Solid-state electron 43:923–929

Rocha JG, Lanceros-Mendez S (2006) 3-D modeling of scintillator-based X-ray detectors. IEEE Sensors J 6:1236–1242

Rocha JG, Ramos NF, Lanceros-Mendez S, Wolffenbuttel RF, Correia JH (2004) CMOS X-rays detector array based on scintillating light guides. Sensors Actuators A 110:119–123

Rocha JG, Dias RA, Goncalves L, Minas G, Ferreira A, Costa CM, Lanceros-Mendez S (2009) X-ray image detector based on light guides and scintillators. IEEE Sensors J 9:1154–1159

Selman J (1994) The fundamentals of X-ray and radium physics, 8th edn. Charles Thomas Publisher, Springfield, p 159

Schumm RH, Wagman DD, Bailey S, Evans WH, Parker VB (1973) National Bureau of Standards (USA). Technical Notes. pp 270-1–270-8

Swank RK (1973) Absorption and noise in X-ray phosphors. J Appl Phys 44:4199–4203

Tate MW, Eikenberry EF, Barna SL, Wall ME, Lowrance JL, Gruner SM (1995) A large-format high-resolution area X-ray detector based on a fiber-optically bonded charge-coupled device (CCD). J Appl Crystallogr 28:196–205

Valentine J, Wehe D, Knoll G, Moss C (1991) Temperature dependence of absolute CsI(Tl) scintillation yield. In: Proceedings of the IEEE Nuclear Science Symposium Conference Record, 176–182

Völklein F, Balles H (1992) A microstructure for measurement of thermal conductivity of polysilicon thin films. J Microelectromechanical Systems 1:193–196

Watanabe S, Ishikawa S, Aono H, Takeda S, Odaka H, Kokubun M, Takahashi T, Nakazawa K, Tajima H, Onishi M, Kuroda Y (2009) High energy resolution hard X-ray and gamma-ray imagers using CdTe diode devices. IEEE Trans Nucl Sci 56:777–782

Workman A, Brettle DS (1997) Physical performance measures of radiographic imaging systems. Dentomaxillofac Radiol 26:139–146

Zentai G, Schieber M, Partain L, Pavlyuchkova R, Proano C (2005) Large area mercuric iodide and lead iodide X-ray detectors for medical and non-destructive industrial imaging. J Crystal Growth 275:e1327–e1331